Journal of Metals, Materials and Minerals, 33(3), 1687, 2023

Synthesis and characterization of electron beam irradiated glutinous rice husk-derived biochar and activated carbon for aqueous electrochemical capacitors

Kittapas KITSANADECHA[1], Charlita SINMAK[1], Patchanan ONCHOMCHAN[1], Kanit HANTANASIRISAKUL[2], Tanagorn KWAMMAN[3,*], Suranan ANANTACHAISILP[1,*]

[1] *Kamnoetvidya Science Academy, 999 Moo 1, Payupnai, Wangchan, Rayong, 21210, Thailand*
[2] *Center of Excellence for Energy Storage Technology (CEST), Department of Chemical and Biomolecular Engineering, School of Energy Science and Engineering, Vidyasirimedhi Institute of Science and Technology, Wangchan Valley, Rayong 21210, Thailand*
[3] *Thailand Institute of Nuclear Technology (Public Organization), 9/9 Moo 7, Saimoon, Ongkharak, Nakhon Nayok, 26120, Thailand*

***Corresponding author e-mail:** suranan.a@kvis.ac.th, tanagorn@tint.or.th
[†]Kittapas Kitsanadecha, Charlita Sinmak, Patchanan Onchomchan contributed equally to this work.

Received date:
17 March 2023
Revised date
20 July 2023
Accepted date:
16 August 2023

Keywords:
Glutinous rice husk;
Electron beam irradiation;
Biochar;
Activated carbon

Abstract

Glutinous rice husk, an abundant agricultural biowaste in Thailand, was pretreated with high energy electron beam irradiation (EBI) at doses of 500 kGy, 1000 kGy, and 1500 kGy prior to fabrication into biochar by carbonization at 500°C under nitrogen atmosphere. The biochar was then treated with KOH and subsequently heated at 800°C, yielding activated carbon (GAC). The physical, chemical, and electrochemical properties of the as-received biochar (GB) and activated carbon (GAC) were investigated. Scanning electron microscopic images (SEM) suggested that biochar irradiated with 1500 kGy (GB-1500) has the highest porosity compared to the other samples. The electrochemical properties of GB and GAC in 3 M H_2SO_4 using a three-electrode system indicated that EBI affects the electrochemical performance of the material. The specific capacitance of GB-1500 (6.15 $F \cdot g^{-1}$ at 0.05 $A \cdot g^{-1}$) is higher than that of the as-received biochar, and the improved performance of the former is potentially due to the formation of structural defects upon irradiation. Finally, we observed that the specific capacitances of the GAC were much higher than those of their corresponding GB with the same irradiation doses, and the capacitances of the GAC decrease with increasing EBI dose.

1. Introduction

Rice husk is a waste byproduct of rice production, and it is generated in large quantities which leads to disposal issues [1]. Most of the techniques used to process rice husk result in the creation of additional waste. These can include but not limited to acidic effluents produced during the cleaning of rice husk, harmful gases released during its incineration, and accumulations of finely dispersed ash [2].

Dried rice husks are composed of 70% to 85% organic matter, which is typically lignin (21%), cellulose (32%), hemicellulose (21%), and other components (20% to 25%) [3]. There is great motivation to use rice husk as a carbon precursor for high-value carbon-based materials due to its high carbon content [4]. Activated carbon has gained much attention recently for various applications due to its high specific surface area, mechanical and chemical stability, and the ability to control the pore size in the material [5].

Recently, there is much interest in activated carbon derived from biowaste, as this feedstock is renewable, abundant, reduces the dependance on fossil fuels, and has a low production cost [4]. As rice husk is a biowaste with little commercial value, this may be an attractive, sustainable material for producing activated carbon [6,7]. Also, this approach could potentially contribute to the solution for reducing in reducing PM 2.5 particles emitted by the incineration of rice husk.

Rice husk, as a lignocellulosic material [8], requires pretreatment to overcome its intrinsic recalcitrant nature [9]. Chemical pretreatment, for instance, using a strong base or a strong acid, are the conventional methods for lignocellulose pretreatment [10]. While these methods produce products with high surface area and high yield, the reagents have a significant environmental footprint [11].

Electron beam irradiation is an upcoming green alternative to chemical pretreatment of materials [12]. Many investigations into this field claim that the mechanical, electronic, and magnetic properties of carbon materials can be modified using high-energy electrons, or photons [13,14]. High energy electrons are obtained and accelerated by an electromagnetic field in an accelerator, and these act to modify the chemical and physical properties of the textile material, or even improve its quality [15]. Additionally, electron beam does not require a radioactive source for generation, unlike gamma-rays, even though they can produce similar effects on carbon materials [16,17]. When the electron beam bombards the material, it breaks the chemical bonds [18] producing free radicals [15] which affect the conductivity of the material [19].

The aim of the present study is to study the effect of electron beam irradiation on the properties of rice husk-derived carbon, including biochar and activated carbon. The effects of electron beam irradiation were studied comparatively at different doses, i.e., 500 kGy, 1000 kGy, and 1500 kGy, with non-irradiated samples used as controls.

2. Experimental

2.1 Materials

Glutinous rice husk was obtained from Surin, Thailand. All chemicals were of analytical grade, and all solutions were prepared with deionized water prior to use.

2.2 Pretreatment

The glutinous rice husk was washed with water to remove dirt and impurities. The rice husk was then dried at 60°C for 48 h then ground and sieved to a particle size of smaller than 200 mesh (74 μm). Next, the prepared husk powder was irradiated with an electron beam (10 MeV, 500 mA) as a pretreatment process at three different doses: 500 kGy, 1000 kGy, and 1500 kGy. The prepared powders were labeled as G-000, G-500, G-1000, and G-1500 according to the dosage used in the irradiation process.

2.3 Preparation of glutinous rice husk-derived biochars

The prepared husk powders were carbonized under a nitrogen atmosphere at 500°C for 1 h with a heating rate of 5°C·min^{-1}. The obtained glutinous rice husk-derived biochars (GB) were labelled as GB-000, GB-500, GB-1000, and GB-1500 according to the radiation dosage for the non-irradiated control, 500 kGy, 1000 kGy, and 1500 kGy, respectively.

2.4 Preparation of glutinous rice husk-derived activated carbons

The glutinous rice husk-derived activated carbon (GAC) was prepared using the following procedure. The rice husk powder was impregnated with 33 wt% KOH and dried at 80°C for 72 h. Then, the dried powder was carbonized at 800°C for 2 h with a heating rate of 5°C·min^{-1}. The GAC sample was then neutralized with 0.1 M H_2SO_4, washed with distilled water, and then dried at 80°C for 24 h. The obtained GAC were labelled as GAC-000, GAC-500, GAC-1000, and GAC-1500 according to the radiation dosage: non-irradiated control, 500 kGy, 1000 kGy, and 1500 kGy, respectively.

2.5 Physio-chemical characterization

The morphology of the GBs and GACs was investigated using a scanning electron microscope (SEM, JEOL JSM-7610F) coupled with energy-dispersive X-ray spectroscopy (EDX). The surface functional groups were identified using Fourier transform infrared spectroscopy (FTIR, Bruker Tensor 27), operating in the range of 4000 cm^{-1} to 500 cm^{-1}. The elemental composition of the surface was determined using X-ray photoelectron spectroscopy (XPS, JPS-9010MC spectrometer, JEOL Ltd.) equipped with a Mg Kα X-ray source. Raman spectroscopy (Raman, XploRA™ PLUS HOLIBA) was conducted over 1000 cm^{-1} to 1800 cm^{-1} at a 532 nm excitation wavelength. Sample crystallinity was investigated using powder X-ray diffraction (XRD, Bruker D8 ADVANCE) with Cu Kα radiation (λ = 1.5406 Å, 40 kV, and 40 mA) in the 2θ range of 10° to 90° with a step size of 0.03°. The specific surface area and pore volume of each sample were obtained by nitrogen adsorption isotherms using BELSORP-mini (Microtrac BEL Crop.) at 77 K. Prior to the adsorption measurements, the samples were degassed, samples were degassed at 90°C for 12 h followed by 300°C for 5 h. The specific surface area of the samples was calculated according to the Brunauer–Emmett–Teller (BET) model. The pore volume was determined by the amount of adsorption at a relative pressure (p/p^o) of about 0.999.

2.6 Electrochemical measurements

The electrochemical performance of the samples was carried out in a three-electrode system. The working electrodes and counter electrodes were prepared by mixing the GBs/GACs, carbon black, and polytetrafluoroethylene (PTFE) at a ratio of 90:5:5 by weight, in ethanol, and the active mass loading was 0.495 mg. After a homogenous dough was formed, it was rolled into a freestanding electrode.

The electrochemical performance of the prepared electrodes was characterized using three-electrode Swagelok type cells in 3 M H_2SO_4 electrolyte. Saturated $Hg/HgSO_4$ was used as a reference electrode, and a Celgard 2400 film served as the separator. The cell setup was connected to an electrochemical station (PGSTAT 302N, Metrohm) for cyclic voltammetry (CV) and galvanostatic charge-discharge (GCD) studies. The specific capacitance (C_p) was calculated using the Equation (1).

$$C_p = \frac{I\Delta t}{m\Delta V} \quad (1)$$

where I is discharge current (A), Δt is the discharge time (s), m is the total mass of the active material (g), and ΔV is the voltage change during discharge (V).

3. Results and discussion

3.1 Physio-chemical properties of GBs and GACs

Raman spectra of GBs is shown in Figure 1(a) and GACs in Figure 1(b). The D band is accounted for the disordered structure of carbon materials while the G band is observed as a result of C=C stretching vibration in the structure [20]. The D and G-bands are noted to be at around 1350 cm^{-1} and 1570 cm^{-1}, respectively [21]. The I_D/I_G ratio (Table 1), which shows the degree of disorderness in GBs, increases as the dose of irradiation is increased. The increase in I_D/I_G ratio shows the effect of EBI on the amount of disordered carbon structure in GB, which indicates the higher surface area of materials [22]. The same trend also applies to GACs where the ratio increases from 0.783 (GAC-000) to 0.990 (GAC-1000). However, the ratio drops to 0.539 for GAC-1500. This can be explained as the effect of EBI which transforms the carbon structure into its nano-crystalline phase and

when the input energy is in excess, it changes the nanocrystallinity structure into the sp^2 amorphous carbon [23,24].

The EDX spectra of GBs and GACs are shown in Figure 2(a-b), respectively. The spectrum shows that GBs contained carbon, oxygen, and silicon as the main composition and a trace of phosphorus and potassium, which came from the nutrients that plants uptake. For GACs, the only elements observed in the spectra are carbon and oxygen.

Figure 3(a-b) shows the XPS spectra of GBs and GACs, respectively. The spectra show that carbon and oxygen are the main elements found, which correlate to the EDX spectra. Moreover, GBs also contained a trace of nitrogen and silicon.

Figure 4(a) shows the FTIR spectra of GBs. All spectra show the absorption band at 1593 cm^{-1} corresponding to the stretching frequency of conjugated ketones, and at 1376 cm^{-1} related to the phenolic -OH bending frequency. Also, at 1070 cm^{-1}, it relates to Si-O-Si asymmetric stretch, which is the signal from the leftover silicon, the main element found in rice husk, in GBs [25].

The nature of carbon and oxygen centers in the samples was examined using XPS. Figure 4(b-c) show the XPS C 1*s* spectra of GB-000 and GB-1500, respectively. The main peak is graphitic carbon (284.6 eV) with small tails of sp^3 carbon (285.6 eV), C-O (286.7 eV), C=O (288.4 eV), and O-C=O (289.1 eV) [26]. The XPS O 1*s* spectra of GB-000 and GB-1500 are also shown in Figure 4(d-e), respectively. Both have the main component of C-O (532.8 eV) with other components of C=O (531.9 eV), O-C=O (531.2 eV), and -OH (533.4 eV) [27]. All the GB samples show similar carbon and oxygen structure.

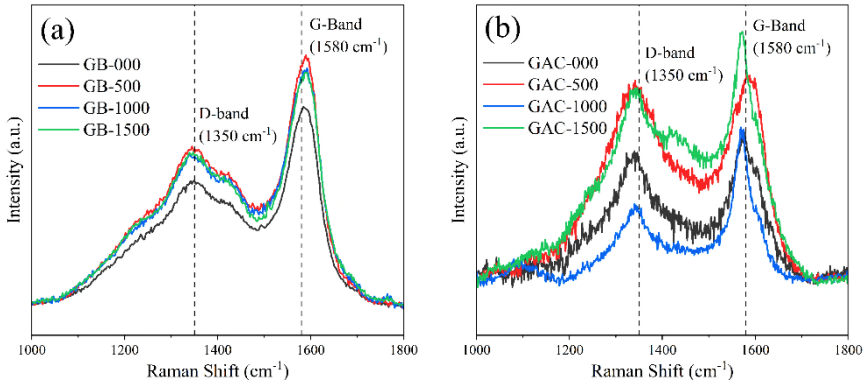

Figure 1. Raman spectra of (a) GBs and (b) GACs.

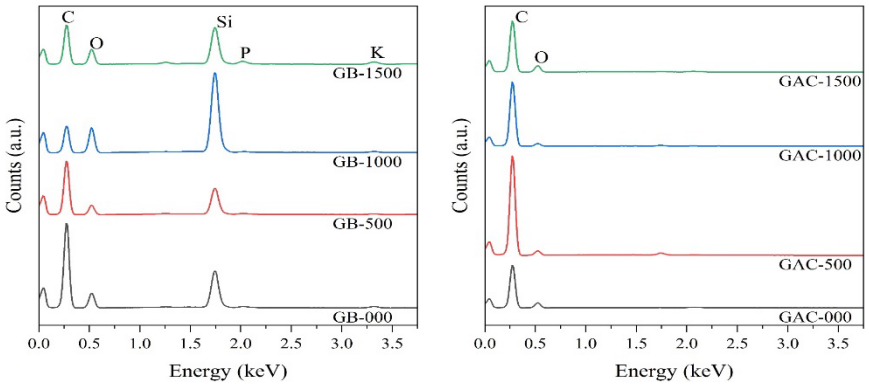

Figure 2. EDX spectra of (a) GBs and (b) GACs.

Table 1. I_D/I_G ratio, specific surface area and pore volume of GBs and GACs.

Sample	I_D/I_G ratio	Specific surface area ($m^2 \cdot g^{-1}$)	Pore volume ($cm^3 \cdot g^{-1}$)
GB-000	0.622	-	-
GB-500	0.627	-	-
GB-1000	0.631	-	-
GB-1500	0.637	-	-
GAC-000	0.783	2068.69	1.038
GAC-500	0.884	814.81	0.597
GAC-1000	0.930	2000.17	1.239
GAC-1500	0.539	1826.61	1.157

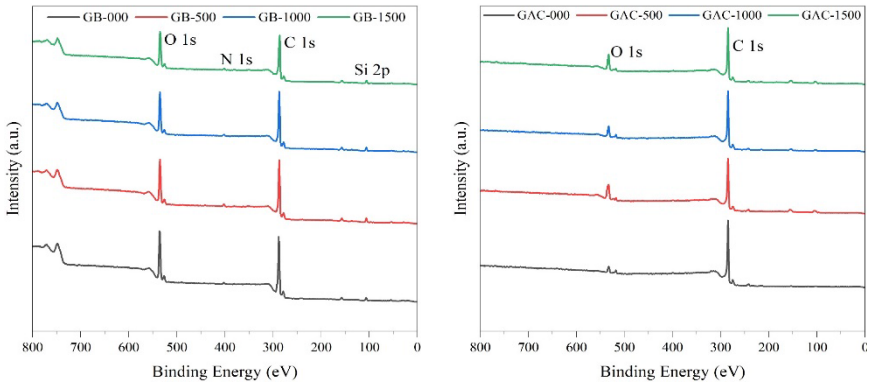

Figure 3. XPS wide scan of (a) GBs and (b) GACs.

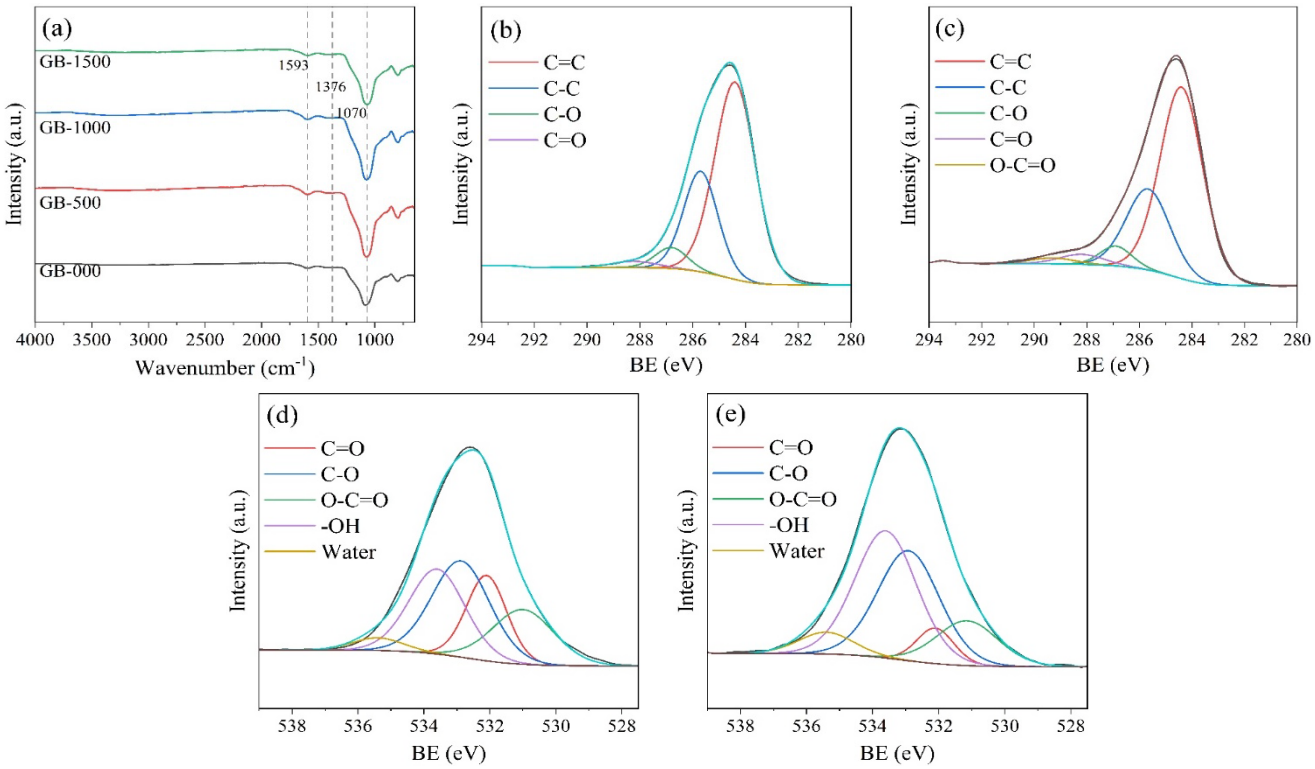

Figure 4. (a) FTIR spectra of GBs. XPS C 1*s* spectra of (b) GB-000 and (c) GB-1500 and XPS O 1*s* spectra of (d) GB-000 and (e) GB-1500.

Figure 5(a-d) shows the SEM images of GB-000, GB-500, GB-1000 and GB-1500. The rough and more spherical surface can be observed only in irradiated samples, which are GB-500, GB-1000 and GB-1500. This indicates the effect of EBI, which cleaves the cellulosic structure of rice husks, on the surface morphology of GB [28]. Moreover, the cleaved structure can self-manufacture into the curly structure corresponding to the spherical structure observed on the surface of irradiated GBs [29].

The XRD patterns of GBs and GACs are shown in Figure 6(a-b), respectively. Two broad peaks at 23° and 45°, were observed in all samples, corresponding to the (002) all samples, correspond to the (002) and (100) planes of graphite, respectively. The similar XRD pattern of each GB samples indicates that all GBs have low crystallinity, which correlates with the I_D/I_G values described earlier. However, the low intensity of (002) peak indicates the increase in structural disorder in GAC-000 and GAC-1000. This may result in higher charge capacity of these materials [30].

The N_2 adsorption-desorption isotherm plots of GACs are shown in Figure 6(c). From the plots, the GAC samples are all having hysteresis loops indicating that they are type IV isotherms, indicating that they contain both micropores and mesopores [31]. Since GAC-000 can adsorb more N_2 over the initial relative pressure range ($p/p^0 < 0.05$), this suggests that it contains the highest number of micropores, followed by GAC-1000 and GAC-1500, respectively [32]. The specific surface area and pore volume of each GACs are shown in Table 1. GAC-000 exhibits the highest specific surface area. This is the result of surface structural breakdown on irradiation [33].

Figure 7(a) shows the FTIR spectra of GACs. All spectra show the absorption band at 3200 cm^{-1} corresponding to the stretching frequency of -OH group, and at 1550 cm^{-1} relating to the aromatic C=C stretching frequency. Also, at 1070 cm^{-1}, there is a strong (C-O-C stretch) peak in every sample. However, the absorption at 1740 cm^{-1} and 1360 cm^{-1}, which correspond to -COO- stretching and -CH_2-

rocking, are found only in the irradiated GACs (GAC-500, GAC-1000, and GAC-1500) [34]. The electron beam irradiation increases the amount of sp^2 carbon as can be seen from the intensity of the peak at 1740 cm^{-1}. This correlates with the results obtained from Raman spectroscopy.

Figure 7(b-c) show the XPS C 1*s* spectra of GAC-000 and GAC-1500, respectively. The main peak is sp^2-bonded carbon (284.6 eV) with small tails of sp^3-bonded carbon (285.6 eV), C-O (286.7 eV), C=O (288.4 eV), and O-C=O (289.1 eV) [26]. The XPS O 1*s* spectra of GAC-000 and GAC-1500 are also shown in Figure 7(d-e), respectively. Both have the main component of C-O (532.8 eV) with other components of C=O (531.9 eV), O-C=O (531.2 eV), -OH (533.4 eV) and water (535.5 eV), which correlate with results from FTIR spectra [27]..

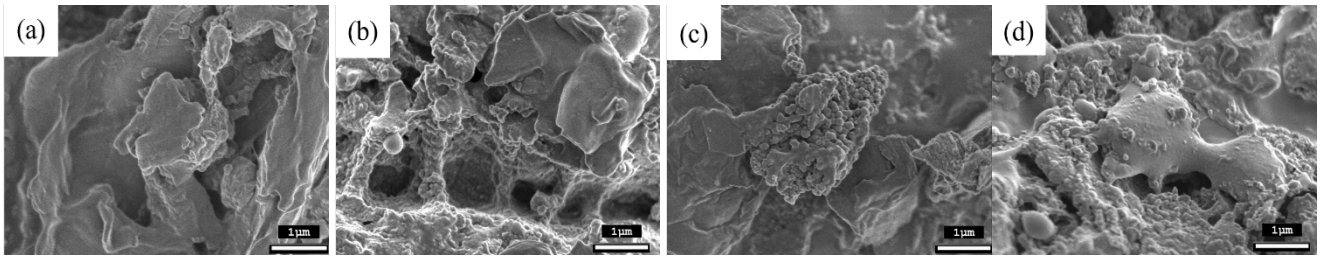

Figure 5. SEM images of (a) GB-000, (b) GB-500, (c) GB-1000 and (d) GB-1500.

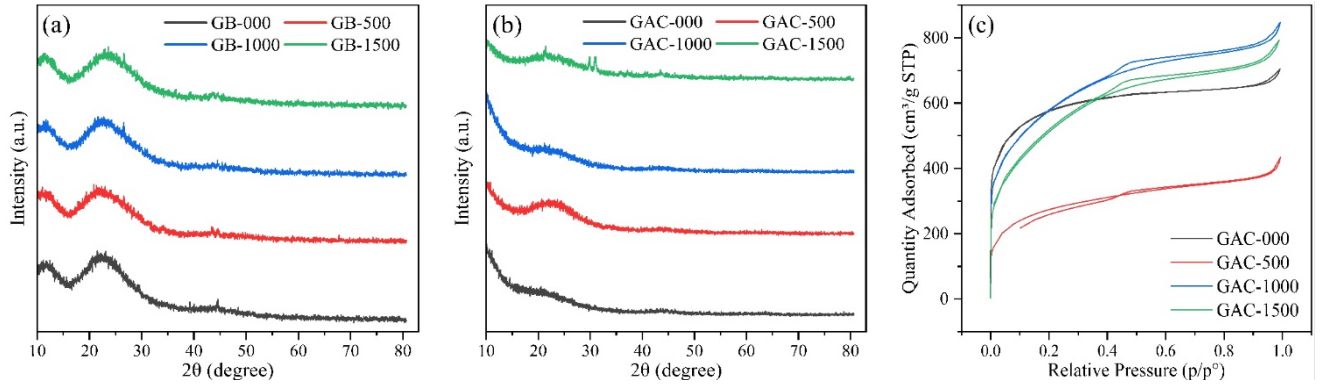

Figure 6. XRD pattern of (a) GBs, (b) GACs, and (c) isotherm plot of GACs.

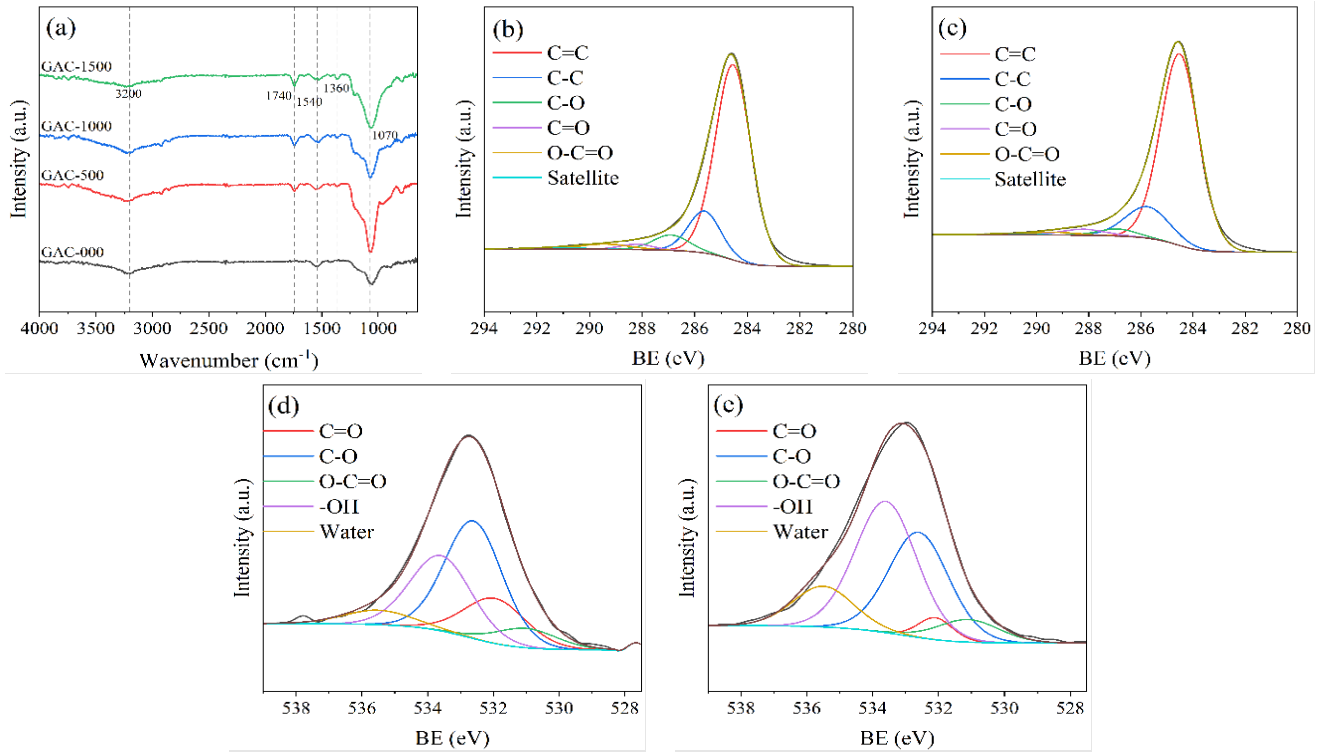

Figure 7. (a) FTIR spectra of GACs, XPS C 1*s* spectra of (b) GAC-000 and (c) GAC-1500 and XPS O 1*s* spectra of (d) GAC-000 and (e) GAC-1500.

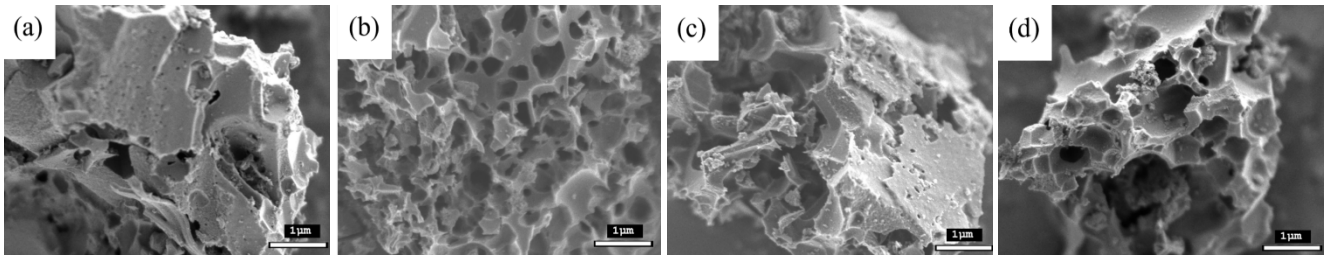

Figure 8. SEM images of (a) GAC-000, (b) GAC-500, (c) GAC-1000, and (d) GAC-1500.

The SEM images of GAC-000, GAC-500, GAC-1000, and GAC-1500 are shown in Figure 8(a-d), respectively. The morphology of every sample shows the more obvious pores and sharper edges compared to GBs as KOH etches rice husk more vigorously than EBI. Moreover, the small spheres found in GBs are not observed in GACs since KOH might completely react with this carbon surface, resulting in breakdown of the spherical structures [35]. Also, the pore size observed is in the same trend as the pore volume acquired from BET calculation

3.2 Electrochemical performances of GBs and GACs

Cyclic voltammetry was done to study the capacitive behavior of the materials. The cyclic voltammograms of GBs are shown in Figure 9(a). Compared to GB-000, GBs that have been through the pretreatment process with EBI have a more supercapacitor-like behavior, as indicated by the quasi-rectangular shapes of their cyclic voltammograms. However, there is also a pseudocapacitive behavior in the GBs as could be determined from both little anodic (GB-500 = -0.025 V; GB-1000 = +0.075 V; GB-1500 = -0.15 V vs $Hg/HgSO_4$) and cathodic peaks (-0.30 V vs $Hg/HgSO_4$). These are the result of redox reactions of oxygen-containing functional groups, e.g., hydroxyl group, as observed in the XPS spectra [36]. In addition, the window shift was observed from GB-000 to the other irradiated GBs, which was caused by the irradiation process.

As indicated in Figure 9(b), all voltammograms of GACs show the characteristic rectangular shape of electrochemical double-layer capacitors (EDLC) [30]. In a similar way to GBs, the anodic (-0.02 V vs $Hg/HgSO_4$) and cathodic (-0.07 V vs $Hg/HgSO_4$) peaks are observed, indicating pseudocapacitive behavior. This helps increase the capacitance of supercapacitors [36].

Next, galvanostatic charge-discharge (GCD) was used to measure the capacitive performance of GBs and GACs. The GCD profiles of GBs are shown in Figure 9(c). The large potential drop in all samples when the measurement started discharging shows the high internal resistance of the materials [36]. The specific capacitance of each sample is shown in Table 2. At current density 0.05 $A \cdot g^{-1}$, GB-000 has the specific capacitance of 1.63 $F \cdot g^{-1}$ and at the same current density, GB-1500 has a specific capacitance of 6.15 $F \cdot g^{-1}$. These results reveal the effect of EBI on the electrochemical performances of GB, suggesting that EBI can potentially be used to increase the electrochemical performance of electrodes made from biochars.

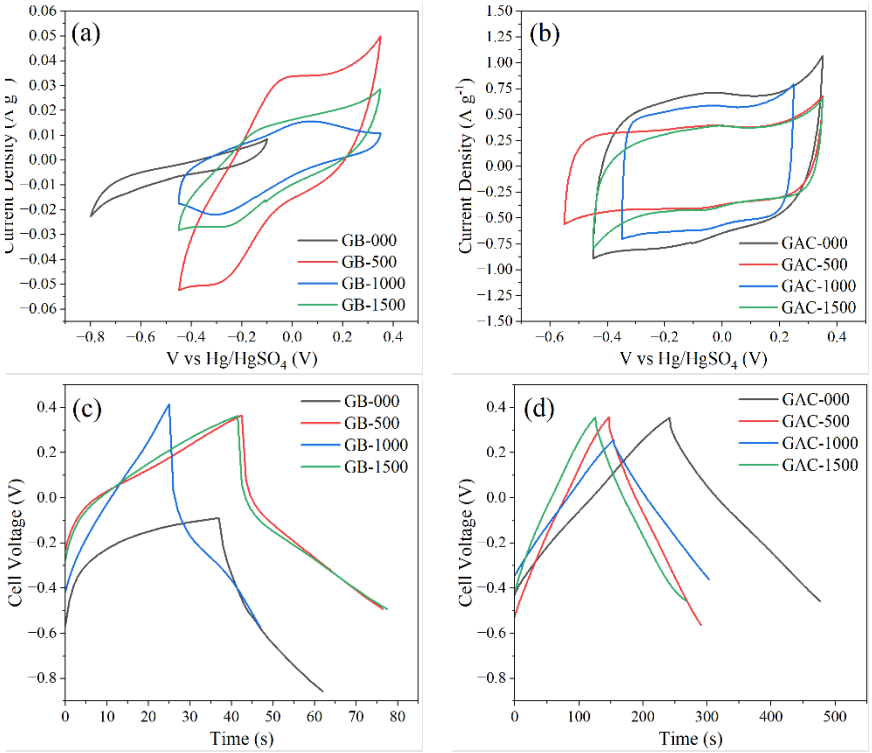

Figure 9. The cyclic voltammograms of (a) GBs and (b) GACs at 5 mV s^{-1} and the GCD profiles of (c) GBs at 0.05 A g^{-1} and (d) GACs at 0.5 A g^{-1}.

Table 2. Specific capacitance of GBs and GACs.

Sample	Specific capacitance ($F \cdot g^{-1}$)	Current density ($A \cdot g^{-1}$)
GB-000	1.63	0.05
GB-500	4.60	0.05
GB-1000	0.58	0.05
GB-1500	6.15	0.05
GAC-000	119.74	0.5
GAC-500	69.35	0.5
GAC-1000	114.77	0.5
GAC-1500	89.09	0.5

Figure 9(d) shows the GCD profiles of GAC samples. All profiles exhibit a triangular shape which indicates that these materials are suitable to be used as supercapacitor electrodes. In contrast to GBs, the calculated specific capacitance shows that GAC-000 exhibits the highest value among GAC samples which is 119.74 F g^{-1} at 0.5 $A \cdot g^{-1}$ while GAC-1500 has the value of 89.09 $F \cdot g^{-1}$ at the same current density, as shown in Table 2. The decreasing trend observed is the result of the same trend seen for the specific surface area of GACs [33]. We speculate that EBI might have destructive effects on the structure and properties of GACs such that it lessens the electro-chemical performances when the materials are used as electrodes [33]. However, the effects of EBI on the structure and properties of GACs or not requires more in-depth investigation, which is beyond the scope of this study.

4. Conclusions

In this study, GBs and GACs were synthesized using different doses of EBI as the pretreatment method. The effect of EBI on electro-chemical performances of supercapacitor electrodes prepared from glutinous rice husk-derived carbon materials was investigated. For GBs, GB-1500 showed the highest specific capacitance of 6.15 $F \cdot g^{-1}$ at 0.05 $A \cdot g^{-1}$ indicating the beneficial effect of EBI on biochar. In contrast, for GACs, GAC-000 exhibited the highest specific surface area among all GAC samples with the value of 2068.69 $m^2 \cdot g^{-1}$ and the specific capacitance of 119.74 $F \cdot g^{-1}$ at 0.5 $A \cdot g^{-1}$ compared to the value of 89.09 $F \cdot g^{-1}$ of GAC-1500. This suggests that although EBI could be used to increase surface area and, hence, charge storage performance of biochar, it shows negative effects on the electrochemical performance after KOH activation. Moreover, KOH activation is still needed to generate activated carbon with suitable electrochemical performance. This study highlights the different effects of EBI on the electrochemical properties of biochar and activated carbon despite derived from the same precursor material. However, further investigation related to the properties of GACs resulted by EBI pretreatment is still required in the future research.

Acknowledgements

The irradiation process was supported by Thailand Institute of Nuclear Technology (Public Organization). The authors acknowledge Centre of Excellence for Energy Storage Technology (CEST), School of Energy Science and Engineering (ESE) and Frontier Research Center (FRC), Vidyasirimedhi Institute of Science and Technology (VISTEC) and Kamnoetvidya Science Academy (KVIS) for providing facilities and technical supports.

References

[1] B. A. Goodman, "Utilization of waste straw and husks from rice production: A review," *Journal of Bioresources and Bioproducts*, vol. 5, no. 3, pp. 143-162, 2020.

[2] S. K. Singh, B. C. Mohanty, and S. Basu, "Synthesis of SiC from rice husk in a plasma reactor," *Bulletin of Materials Science*, vol. 25, pp. 561-563, 2002.

[3] L. Shrestha, M. Thapa, R. Shrestha, S. Maji, R. Pradhananga, and K. Ariga, "Rice husk-derived high surface area nanoporous carbon materials with excellent iodine and methylene blue adsorption properties," *C-Journal of Carbon Research*, vol. 5, no. 1, p. 10, 2019.

[4] S. Saini, P. Chand, and A. Joshi, "Biomass derived carbon for supercapacitor applications: Review," *Journal of Energy Storage*, vol. 39, p. 102646, 2021.

[5] G. Zhang, Y. Chen, Y. Chen, and H. Guo, "Activated biomass carbon made from bamboo as electrode material for super-capacitors," *Materials Research Bulletin*, vol. 102, pp. 391-398, 2018.

[6] C. A. M. Moraes, I. J. Fernandes, D. Calheiro, A. G. Kieling, F. A. Brehm, M. R. Rigon, J. A. Berwanger Filho, I. A. H. Schneider, and E. Osorio, "Review of the rice production cycle: By-products and the main applications focusing on rice husk combustion and ash recycling," *Waste Management & Research: The Journal for a Sustainable Circular Economy*, vol. 32, no. 11, pp. 1034-1048, 2014.

[7] J. Paduraksa, M. Luthfi, A. Verdianto, A. Subhan, W. B. Widayatno, B. Prihandoko, E. Kartini, and C. Hudaya, "Preparation of activated carbon derived from water hyacinth as electrode active material for Li-Ion Supercapacitor," *Materials Science Forum*, vol. 1000, pp. 50-57, 2020.

[8] H. Chen, W. Wang, J. C. Martin, A. J. Oliphant, P. A. Doerr, J. F. Xu, K. M. DeBorn, C. Chen, and L. Sun, "Extraction of lignocellulose and synthesis of porous silica nanoparticles from Rice Husks: A comprehensive utilization of rice husk biomass," *ACS Sustainable Chemistry & Engineering*, vol. 1, no. 2, pp. 254-259, 2012.

[9] N. Ali, Q. Zhang, Z.-Y. Liu, F.-L. Li, M. Lu, and X.-C. Fang, "Correction to: Emerging technologies for the pretreatment of lignocellulosic materials for bio-based products," *Applied Microbiology and Biotechnology*, vol. 104, no. 11, pp. 5159-5159, 2020.

[10] M. Taherzadeh, and K. Karimi, "Pretreatment of lignocellulosic wastes to improve ethanol and biogas production: A Review,"

International Journal of Molecular Sciences, vol. 9, no. 9, pp. 1621-1651, 2008.

[11] S. S. Hassan, G. A. Williams, and A. K. Jaiswal, "Emerging technologies for the pretreatment of Lignocellulosic Biomass," *Bioresource Technology*, vol. 262, pp. 310-318, 2018.

[12] U. Henniges, M. Hasani, A. Potthast, G. Westman, and T. Rosenau, "Electron beam irradiation of cellulosic materials—opportunities and limitations," *Materials*, vol. 6, no. 5, pp. 1584-1598, 2013.

[13] E. Adhamash, R. Pathak, Q. Qiao, Y. Zhou, and R. McTaggart, "Gamma-radiated biochar carbon for improved supercapacitor performance," *RSC Advances*, vol. 10, no. 50, pp. 29910-29917, 2020.

[14] R. Sindhu, P. Binod, and A. Pandey, "Biological Pretreatment of lignocellulosic biomass – an overview," *Bioresource Technology*, vol. 199, pp. 76-82, 2016.

[15] T. Abou Elmaaty, S. Okubayashi, H. Elsisi, and S. Abouelenin, "Electron beam irradiation treatment of textiles materials: A review," *Journal of Polymer Research*, vol. 29, no. 4, 2022.

[16] M. R. Cleland, "Industrial applications of electron accelerators," *CAS - CERN Accelerator School: small accelerators*, pp. 383-416, 2006.

[17] J.-il Choi, J.-H. Kim, K.-W. Lee, B.-S. Song, Y. Yoon, M.-W. Byun, and J.-W. Lee, "Comparison of gamma ray and electron beam irradiations on the degradation of carboxymethylcellulose," *Korean Journal of Chemical Engineering*, vol. 26, no. 6, pp. 1825-1828, 2009.

[18] M. Ghaffour, A. Abdellaoui, M. Bouslama, A. Ouerdane, and Y. Al-Douri, "Study by AES and EELS of InP, InSb, $InPO_4$ and $In_xGa_{1-x}As$ submitted to electron irradiation," *Surface Review and Letters*, vol. 19, no. 01, p. 1250002, 2012.

[19] J. M. Pochan, H. W. Gibson, and J. Harbour, "The effect of a free radical quencher on the conductivity, oxidative stability and free radical population of poly(1,6-heptadiyne)," *Polymer*, vol. 23, no. 3, pp. 435-438, 1982.

[20] E. Y. Teo, L. Muniandy, E.-P. Ng, F. Adam, A. R. Mohammed, R. Jose, and K. F. Chong., "High surface area activated carbon from rice husk as a high performance supercapacitor electrode," *Electrochimica Acta*, vol. 192, pp. 110-119, 2016.

[21] Y. Wang, D. C. Alsmeyer, and R. L. McCreery, "Raman spectroscopy of carbon materials: Structural basis of observed spectra," *Chemistry of Materials*, vol. 2, no. 5, pp. 557-563, 1990.

[22] X. Wei, J.-S. Wei, Y. Li, and H. Zou, "Robust hierarchically interconnected porous carbons derived from discarded Rhus typhina fruits for ultrahigh capacitive performance supercapacitors," *Journal of Power Sources*, vol. 414, pp. 13-23, 2019.

[23] D. Teweldebrhan and A. A. Balandin, "Modification of graphene properties due to electron-beam irradiation," *Applied Physics Letters*, vol. 94, no. 1, 2009.

[24] M. Z. Iqbal, A. Kumar Singh, M. W. Iqbal, S. Seo, and J. Eom, "Effect of e-beam irradiation on graphene layer grown by chemical vapor deposition," *Journal of Applied Physics*, vol. 111, no. 8, p. 084307, 2012.

[25] N. Hossain, S. Nizamuddin, G. Griffin, P. Selvakannan, N. M. Mubarak, and T. M. Mahlia, "Synthesis and characterization of rice husk biochar via hydrothermal carbonization for wastewater treatment and biofuel production," *Scientific Reports*, vol. 10, no. 1, 2020.

[26] W. Tian, Q. Gao, Y. Tan, K. Yang, L. Zhu, C. Yang, and H. Zhang, "Bio-inspired beehive-like hierarchical nanoporous carbon derived from bamboo-based industrial by-product as a high performance supercapacitor electrode material," *Journal of Materials Chemistry A*, vol. 3, no. 10, pp. 5656-5664, 2015.

[27] D. Liu, W. Zhang, H. Lin, Y. Li, H. Lu, and Y. Wang, "Hierarchical porous carbon based on the self-templating structure of rice husk for high-performance supercapacitors," *RSC Advances*, vol. 5, no. 25, pp. 19294-19300, 2015.

[28] U. Gryczka, W. Migdal, D. Chmielewska, M. Antoniak, W. Kaszuwara, A. Jastrzebska, and A. Olszyna, "Examination of changes in the morphology of lignocellulosic fibers treated with e-beam irradiation," *Radiation Physics and Chemistry*, vol. 94, pp. 226–-30, 2014.

[29] S. Gupta, and R. J. Patel, "Changes in the vibrational modes of carbon nanotubes induced by electron-beam irradiation: Resonance Raman spectroscopy," *Journal of Raman Spectroscopy*, vol. 38, no. 2, pp. 188-199, 2007.

[30] D. Yan, L. Liu, X. Wang, K. Xu, and J. Zhong, "Biomass-derived activated carbon nanoarchitectonics with Hibiscus flowers for high-performance supercapacitor electrode applications," *Chemical Engineering & Technology*, vol. 45, no. 4, pp. 649-657, 2022.

[31] T. C. Chandra, M. M. Mirna, J. Sunarso, Y. Sudaryanto, and S. Ismadji, "Activated carbon from Durian Shell: Preparation and characterization," *Journal of the Taiwan Institute of Chemical Engineers*, vol. 40, no. 4, pp. 457-462, 2009.

[32] P. Schneider, "Adsorption isotherms of microporous-mesoporous solids revisited," *Applied Catalysis A: General*, vol. 129, no. 2, pp. 157-165, 1995.

[33] M.-J. Jung, M.-S. Park, and Y.-S. Lee, "Effects of e-beam irradiation on the chemical, physical, and electrochemical properties of activated carbons for electric double-layer capacitors," *Journal of Nanomaterials*, vol. 16, no. 1, pp. 201, 2015.

[34] S. Sathyamoorthi, N. Phattharasupakun, and M. Sawangphruk, "Environmentally benign non-fluoro deep eutectic solvent and free-standing rice husk-derived bio-carbon based high-temperature supercapacitors," *Electrochimica Acta*, vol. 286, pp. 148-157, 2018.

[35] J. Wang, and S. Kaskel, "KOH activation of carbon-based materials for energy storage," *Journal of Materials Chemistry*, vol. 22, no. 45, p. 23710, 2012.

[36] W. Zhang, N. Lin, D. Liu, J. Xu, J. Sha, J. Yin, X. Tan, H. Yang, H. Lu, and H. Lin, "Direct carbonization of rice husk to prepare porous carbon for supercapacitor applications," *Energy*, vol. 128, pp. 618-625, 2017.

[37] M. D. Stoller, S. Park, Y. Zhu, J. An, and R. S. Ruoff, "Graphene-based ultracapacitors," *Nano Letters*, vol. 8, no. 10, pp. 3498-3502, 2008.